Optical properties of solution-chemically derived thin film Ni–Al_2O_3 composites and Si, Al and Si–Ti oxides

2006 J. Phys.: Condens. Matter 18 7737

(http://iopscience.iop.org/0953-8984/18/32/021)

INSTITUTE OF PHYSICS PUBLISHING JOURNAL OF PHYSICS: CONDENSED MATTER

J. Phys.: Condens. Matter **18** (2006) 7737–7750 doi:10.1088/0953-8984/18/32/021

Optical properties of solution-chemically derived thin film Ni–Al_2O_3 composites and Si, Al and Si–Ti oxides

Tobias K Boström and Ewa Wäckelgård

Division of Solid State Physics, Department of Engineering Sciences, Uppsala University, PO Box 534, Uppsala, SE-751 21, Sweden

E-mail: Tobias.Bostrom@Angstrom.uu.se

Received 28 April 2006, in final form 13 July 2006
Published 31 July 2006
Online at stacks.iop.org/JPhysCM/18/7737

Abstract

The refractive index in the wavelength range 350–2500 nm of solar absorbing and anti-reflecting thin films was determined from reflectance and transmittance measurements. Knowing the refractive indices of such films was important when designing an optimized spectrally selective surface for solar thermal usage. The absorbing thin films were made of nickel–alumina composites with a nickel content varying from 20 to 80%. The anti-reflecting films were made of silica, hybrid-silica, alumina and silica–titania composites.

(Some figures in this article are in colour only in the electronic version)

1. Introduction

This work is related to preceding studies of highly spectrally selective and durable solution-chemically derived solar thermal absorbers. Advantages of this novel technique to manufacture thin film nickel–alumina composites are that it is simple and easy to control, the coating can be manufactured under ambient pressure conditions, and the process is low in material consumption. The method seems promising and could hopefully reduce production costs for spectrally selective absorbers and hence make them less expensive and more readily available. The produced selective absorber belongs to a group of absorbers called metal–dielectric composite/metal tandem, which normally consists of selectively absorbing thin films with metal nanoparticles embedded in a dielectric matrix applied on a highly reflecting metal surface [1]. The studied selectively absorbing films are composed of nickel nanoparticles in a surrounding dielectric matrix of alumina, with varying proportions. In this case the optimized solar absorber is constructed out of an aluminium substrate that is coated with three layers: a highly absorbing nickel–alumina film at the base, a medium absorbing nickel–alumina film in the middle and an anti-reflecting (AR) film at the top. The AR materials were made from silica, hybrid-silica or silica–titania mixtures. The solution-chemical routes to produce these materials are described in previous papers [2, 3].

In order to design the optimal three-layer combination a thin film simulation program CODE (Coating Designer) [4] was utilized. But to be able to use the program the optical constants of the thin film materials in question have to be known. Since the selectively absorbing nickel–alumina material is newly invented there exist no refractive index data on it. Wavelength dependent refractive index data on silica–titania materials were also not to be found. The program can however use empirical reflectance and transmittance measurement data of thin films coated on glass substrates to fit the corresponding refractive index [5]. The derivation of optical constants of transparent or semitransparent thin films on a transparent substrate is a well known method from a theoretical and practical point of view [6]. Semitransparent thin selectively absorbing films of about 50–100 nm in thickness consisting of different volume percentages of nickel, ranging from 0 to 80%, were coated on glass and the reflectance and transmittance spectra between 350 and 2500 nm were measured. Equally thin AR films made of silica, hybrid-silica and silica–titania mixtures were also characterized using the same method. Silica is well known to be a very resilient but static material. In order to make silica more flexible an organic compound can be incorporated into the structure and then the resulting material is called hybrid-silica [7].

A selective absorber is characterized by the two parameters normal solar absorptance and normal thermal emittance [8]. The solar absorptance should ideally be 1, meaning that all solar energy is absorbed. The thermal emittance value should ideally be 0, meaning that no heat is lost through thermal radiation from the absorber surface. The optimized solution-chemically derived patented selective absorber achieves a very high efficiency, a normal solar absorptance of 0.97 and a normal thermal emittance of 0.05 [3].

This paper focuses on deriving the optical properties of the absorbing and AR thin film materials which were necessary to be able to design an optimized three-layer nickel–alumina absorber. The design of the optimized three-layer absorber was published earlier [3] but the optical constants on which the optimized absorber was based were not, and the purpose of this paper is thus to publish the optical constants of the novel nickel–alumina composite. The AR silica/titania mixture material is not novel but there exist no published wavelength dependent refractive index data and thus we publish these data as well. The refractive index of silica (and hybrid-silica) is of course well known but is included for comparison and discussion.

2. Method

Several approaches can be pursued [9] but the method used in this paper was to simultaneously fit reflectance and transmittance spectra using a thin film fitting program. In this case the program utilizes measured reflectance and transmittance spectra of thin films coated on transparent 500 μm thick, type 7059 Corning glass substrates to fit the corresponding complex refractive index. In order to avoid a sharp absorption peak at $\lambda < 320$ nm originating from the Corning glass substrate, the fitting of all prepared samples was performed in the wavelength interval 350–2500 nm. White light interferometry shows that the Corning glass has an rms value of 0.85 nm.

The normal reflectance and transmittance was measured by a Perkin-Elmer Lambda 900 spectrophotometer equipped with an integrating sphere of diameter 150 mm, and a circular beam entrance with reflectance and transmittance sample ports of 19 and 25 mm respectively. Spectralon was used as a reference substrate. The measurement reproducibility of the Lambda 900 is within 99.8%. Other measurement errors deriving from the geometry of the sphere and the surface structure of the sample are less than 0.5%.

Roughness and reference thickness measurements of the thin film samples were made using a White Light Interferometer (WLI) of type Wyko NT-1100. An area of about 2×2 mm^2 could be viewed when using the 2.5$\times$ objective.

2.1. Dispersion models

The first step in order to derive the optical constants using a refractive index fitting program is to define dispersion models for the various studied materials, including the glass substrate.

2.1.1. Corning glass. The decaying Cauchy dispersion model was used for the substrate glass [10]; see equation (1). By avoiding absorption peaks in the infrared and ultraviolet from the crystalline silica and only looking in the interval 350–2500 nm, ε_2 is equal to 0.

$$\varepsilon_1 = c_1 + \frac{c_2}{\lambda^2}. \tag{1}$$

The variable c_1 represents the constant level in the long wavelength range of the interval, and c_2 fits the decay rate of ε_1. The Corning glass substrate was hence fitted using two free variables, c_1 and c_2; the thickness d was fixed to 500 μm.

2.1.2. Oxides. We are aware of that we use a mathematical model (equation (2)) where ε_1 and ε_2 are independent of each other. These models are applicable when analysing the optical properties in the wavelength side of strong absorption due to interband transitions. For the materials in question the long wavelength range is $\lambda > 300$ nm.

The dispersion model, see equation (2), for the alumina, silica, hybrid-silica, and two silica–titania oxide composites is not based on physically describing model; it is rather an empirical mathematical dispersion model [5]. Equation (2) is very similar to the widespread and accepted Cauchy model which also utilizes a non-correlated ε_1 and ε_2 model. The mathematical model presented here is motivated since it gives a better fit compared to the Cauchy model. These models are applicable when analysing the optical properties for the materials in question in the long wavelength side of strong absorption related to interband transitions, that is for $\lambda > 300$ nm. When deriving the refractive index in such a narrow wavelength interval, 350–2500 nm, it is very difficult to make a reliable Kramers–Krönig transformation.

$$\varepsilon_1 = c_1 \exp((350 - \lambda)/c_2) + c_3. \tag{2a}$$

$$\varepsilon_2 = c_4 \exp((350 - \lambda)/c_5) + c_6. \tag{2b}$$

The variables c_1 and c_4 fit the function values for ε_1 and ε_2 respectively, at a wavelength λ between 350 and 2500 nm. c_2 and c_5 fit the decay rates of each function. c_3 and c_6 are the constant levels in the long wavelength range of the interval. The previously derived refractive index for the Corning glass according to equation (1) was imported and added as the base substrate when determining the refractive index of the dielectric oxides. These oxides were thus fitted using seven free variables, c_1–c_6 and the thickness, d.

2.1.3. Nickel–alumina composite. Scanning and transmission electron microscopy (SEM and TEM) studies have shown that the nickel particle size is of the order of 5–10 nm [2, 3]. The aggregates are thus much smaller than the wavelength of the light in the studied wavelength interval. The alumina and nickel composite could consequently be considered as an effective medium component according to the Bruggeman model [11]:

$$(1 - f)\frac{\varepsilon_{Al_2O_3} - \varepsilon_{eff}}{\varepsilon_{Al_2O_3} + 2\varepsilon_{eff}} + f\frac{\varepsilon_{Ni} - \varepsilon_{eff}}{\varepsilon_{Ni} + 2\varepsilon_{eff}} = 0 \tag{3}$$

where ε_{Ni} is the complex dielectric function for nickel, taken from the literature [12], and $\varepsilon_{Al_2O_3}$ is the complex dielectric function for alumina. Note that the derived refractive index for pure alumina was not used; instead the alumina in each nickel–alumina composite was refitted according to equation (2). The effective medium dielectric function of the composite film

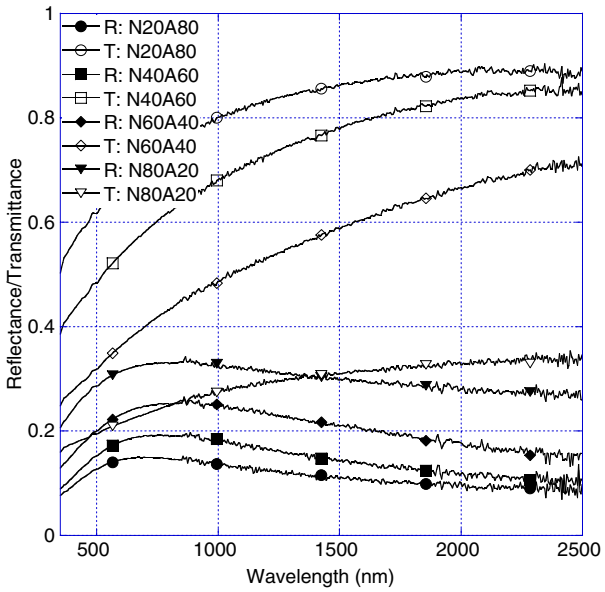

Figure 1. Reflectance and transmittance example graphs of the nickel–alumina composites studied.

is denoted ε_{eff} and the volume fraction nickel is denoted f. The previously derived refractive index for the Corning glass according to equation (1) was however also imported here and added as the base substrate. The nickel–alumina composite was consequently the most complex, being fitted with eight free variables, c_1–c_6, d and the volume fraction, f.

2.2. Reflectance and transmittance spectra

Reflectance and transmittance spectra were measured for the semitransparent thin films coated on Corning glass. The films were either selectively absorbing thin films consisting of different volume percentages of nickel ranging from 20 to 80% or AR films made of silica, hybrid-silica, alumina and silica–titania mixtures. Examples of reflectance and transmittance graphs of nickel–alumina films can be seen in figure 1.

2.3. Fitting procedure

Reflectance and transmittance data were imported into the fitting program (CODE). The program utilizes a least deviation method to calculate the free variables. After reasonable start values are found manually, an automatic fit function can be activated. The automatic parameter fit for each parameter set is done by a routine that utilizes a downhill simplex algorithm. The downhill simplex method is a simple but stable algorithm that minimizes the sum of squared errors, i.e. the fit deviation [13, 14].

In almost all cases this method will find the next local minimum of the fit deviation. There is, however, no guarantee that this is the global minimum as well. The risk of getting an incorrect solution was minimized by selecting good starting values close to the global minimum and by inspecting the final solution carefully. A list of the fitted parameter values can be found in table A.1 in the appendix (the nomenclature N40A60 is explained in the caption). An example of fitted reflectance and transmitted data for an N40A60 film can be seen in figure 2.

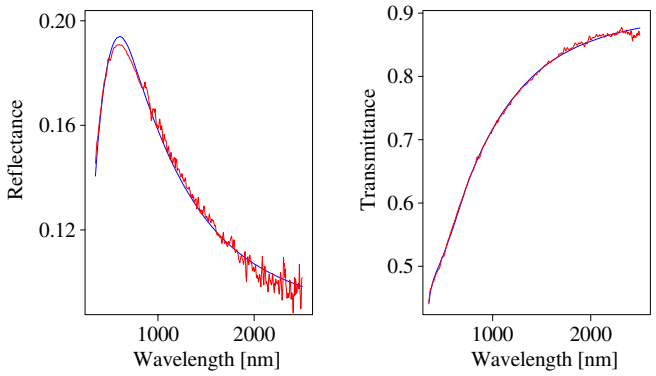

Figure 2. Fitted reflectance and transmitted data for a 56 nm N40A60 film: the jagged line represents the spectrophotometer data and the smooth line the fit. Observe the high resolution scale especially on the reflectance graph.

Table 1. Thickness (d) and volume fraction (f) of nickel derived from the fitting program for the various thin films studied. S = silica, HS = hybrid-silica (80 mol% silica and 20 mol% hybrid-silica), A = alumina, SxxTyy = silica–titania (xx mol% silica and yy mol% titania), NxxAyy = nickel–alumina (xx vol% nickel and yy vol% alumina). The subscript refers to the sample number (i.e. for N40A60 there are 3 samples).

Material	S/HS	A	S70T30	S50T50	N20A80	N40A60	N60A40	N65A35	N80A20
d_1 (nm)	80	35	139	97	45	44	47	60*	50
f_1 (%)	—	—	—	—	2.8	4.7	9.0	16.4	33.9
d_2 (nm)	90*	52	242	177	55	56	70	72*	55*
f_2 (%)	—	—	—	—	3.1	4.8	9.0	19.2	38.7
d_3 (nm)	90*				82	79		115*	95*
f_3 (%)	—				2.6	3.5		15.9	32.9
d_4 (nm)	99								
f_4 (%)	—								

3. Experimental work

The solution-chemical route for the alumina and a nickel precursor solution is under a patenting process and can therefore not be described. The silica and hybrid-silica sol–gel production routes originate from a paper by Tadanaga *et al* [7]. The silica–titania mixtures were produced with a sol–gel technique originating from Dawnay *et al* [15]. The exact recipes that were used in this paper are described in [3]. The spin coated films are very uniform and homogenous with an rms value of around 3 nm.

4. Results

4.1. Volume fraction and thickness

The volume fractions found by the fitting program are presented in table 1. CODE in this case uses the Bruggeman approximation and the volume fraction according to equation (3). At least two samples with varying thicknesses were prepared for all material compositions studied; see table 1. The refractive index was obtained through the fitting process for each individual

sample. The error limits, shown as grey lines in the graphs, were derived from calculating the standard deviation between the two to four samples for each material.

Reference thickness measurements were performed using the WLI. The WLI thicknesses obtained normally correlated very well (±5 nm) with the derived thicknesses from the thin film program. There was however an exception for silica/hybrid-silica samples and for samples with 65% nickel or more: here CODE typically overestimates the thicknesses by up to 20%. Thicknesses in table 1 with an asterisk indicate that the WLI obtained value was used and then fixed when deriving the refractive index.

4.2. Corning 7059 glass

The refractive index was found to be 1.57 at 350 nm, 1.55 at 436 nm, 1.53 at 644 nm and 1.52 at 2500 nm. The imaginary part is equal to zero over the whole spectrum. The tabled refractive index of crystalline type αSiO_2 is equal to 1.57 at 350 nm, 1.55 at 436 nm, 1.54 at 644 nm and 1.51 at 2500 nm [12]. The alkali level in the 7059 Corning glass is less than 0.3%, making it very close to pure crystalline SiO_2. Vin Karola Instruments state a refractive index of the 7059 Corning glass of 1.54 at 436 nm and 1.53 at 644 nm [16]. The refractive index found in this study for 7059 Corning glass thus matches the tabled and stated values very well.

Table A.1 in the appendix shows the parameter values from the dispersion model used, equation (1). These values were fixed in the following fits having the Corning glass as substrate.

4.3. Nickel–alumina

Table A.1 in the appendix shows the parameter values c_1–c_6 for the alumina related to the used dispersion model; see equation (2). All samples in this section were annealed to 550 °C.

4.3.1. Pure alumina. Shamala *et al* have determined the real part of the refractive index to be 1.61 and 1.58 at 500 nm for an evaporated and a spray-pyrolysed amorphous alumina thin film, respectively [17]. Shamala *et al* have however not stated or mentioned anything about the imaginary part. Eriksson *et al* have investigated amorphous evaporated alumina, also only for the real part of the refractive index but in the interval 400–2100 nm, where the refractive index was measured to be 1.62 and 1.57 at 400 and 2100 nm, respectively [18]. The real part of the refractive index for the solution-chemically derived alumina films in this study seen in figure 3 is 1.64 ± 0.02 at 400 nm, 1.63 ± 0.02 at 500 nm and 1.58 at 2100 nm. The corresponding values for the imaginary part seen in figure 4 are 0.05 ± 0.02, 0.03 ± 0.01 and 0.00. Previous x-ray diffraction studies have shown that the solution-chemically derived alumina is amorphous [2].

4.3.2. Nickel–alumina composites. As the nickel content gradually increases, both the real and imaginary refractive index increase. The nickel nanoparticles are heavily absorbing, especially in the solar spectrum. The extinction coefficient exhibits a peak around 500 nm which originates from the absorptive nickel nanoparticles. The absorption peak, seen in figure 4, shifts from 400 nm for samples with 20% nickel to 600 nm for samples with 65% nickel. This shift in the absorption peak can be derived from the Bruggeman formula and has been reported earlier [19]. The composite can be characterized as a dielectric material with a decreasing complex refractive index with wavelength in the near-infrared wavelength range for nickel contents between 20 and 60%; see figure 4.

Composites with 65% nickel are on the verge of becoming metallic, still showing a decrease in k but now with a steady increase in n in the near-infrared wavelength range; see figures 3 and 4. For composites with 80% nickel, see figure 5, k as well as n increases with increasing wavelength, implying an optically metallic behaviour; there is conclusively a gradual

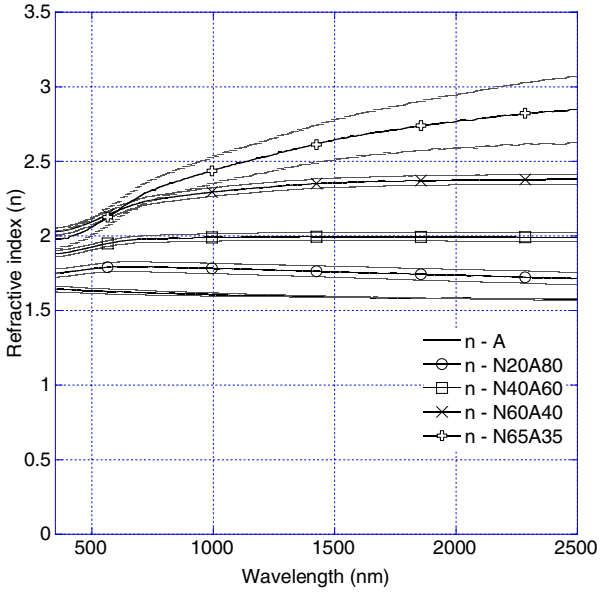

Figure 3. The real part (n) of the average refractive index of pure alumina (A) to 65%nickel–35%alumina (N65A35) thin film samples; the grey lines represent the standard deviation.

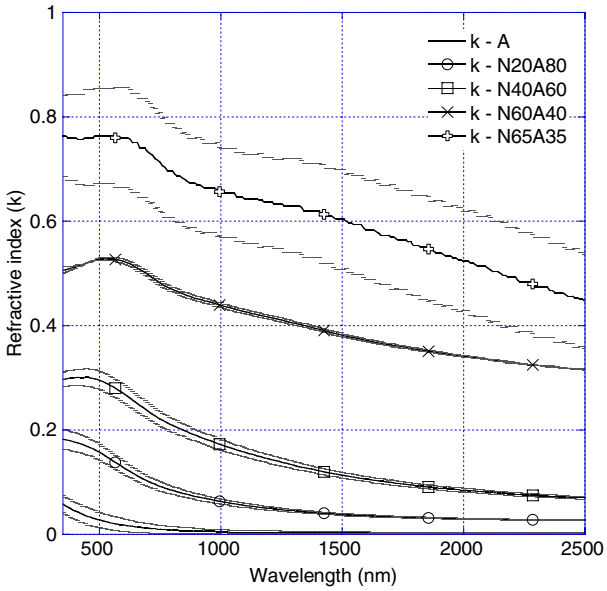

Figure 4. The imaginary part (k) of the average refractive index of pure alumina (A) to 65%nickel–35%alumina (N65A35) thin film samples; the grey lines represent the standard deviation.

transition to a more metallic behaviour of the nickel–alumina composite somewhere between a nickel percentage of 65–80. However, an absorption bulge can still be seen but at 700 nm, see figure 5, for the 80% nickel samples, which indicates that the nickel particles are still separated and have not agglomerated completely. Transmission electron microscopy studies pending

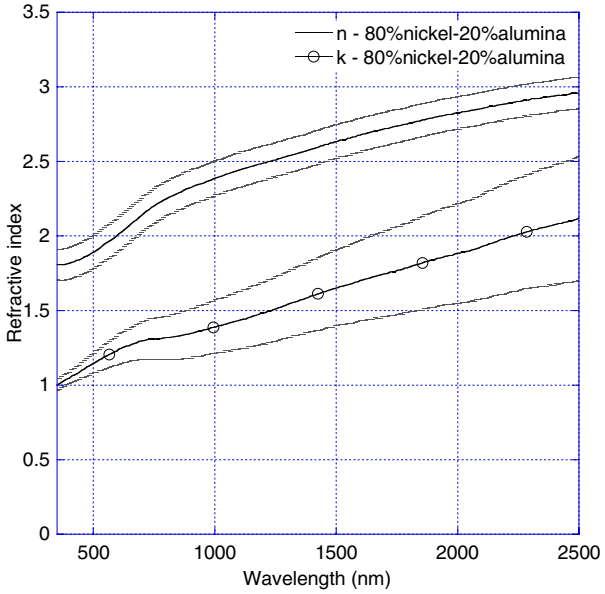

Figure 5. Average refractive index of N80A20 thin film samples; the grey lines represent the standard deviation.

publication support this assumption [20]. The TEM images show separated particles even at a nickel content of 80%.

Figure 6 shows the real refractive index at 2500 nm, which corresponds to $\varepsilon(\infty)$ in the dispersion model, as a function of solution volume nickel content for the dielectric nickel–alumina composites having a nickel content of 0–60%. Samples with 65 and 80% nickel were not included since, because of the high nickel content, they appear more metallic rather than dielectric.

4.4. Anti-reflection oxides

Table A.1 in the appendix shows the parameter values c_1–c_6 for the oxides related to the dispersion model used; see equation (2).

4.4.1. Silica and hybrid-silica. The refractive index of the amorphous sol–gel derived thin film silica and hybrid-silica annealed to 400 °C in this study is 1.42 ± 0.02, and is constant over the whole spectrum (350–2500 nm). The silica and hybrid-silica films showed no absorption. The refractive index of densified amorphous organic-free thin film silica at 633 nm is 1.46 according to Seco *et al* [21]. The same paper reports 1.39 ± 0.01 at 633 nm and a porosity of $13 \pm 1.0\%$ for their sol–gel derived silica thin films.

4.4.2. Silica–titania composites. The S70T30 and S50T50 processing method originates from Dawnay *et al* [15], who found that the resulting films were fully densified providing that the samples were subjected to a rapid heating treatment. Dawnay *et al* did not state any refractive index. Brusantin *et al* [22], however, stated values in the range of 1.61–1.63 at 633 nm for an S70T30 thin film. No report on the refractive index of S50T50 was found.

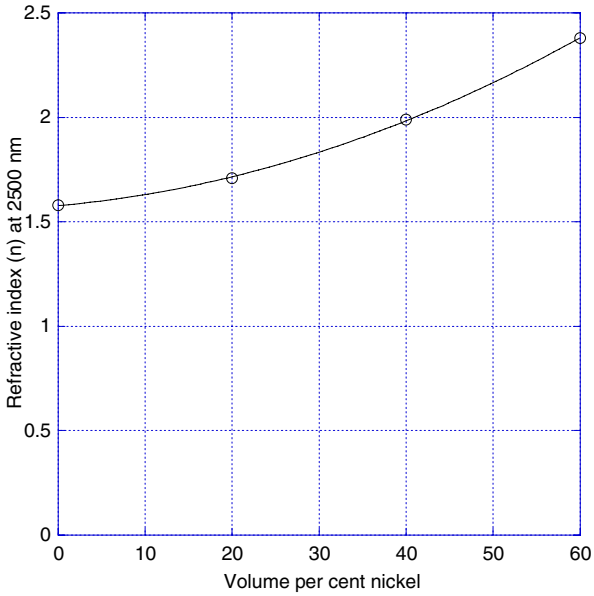

Figure 6. The refractive index n value at 2500 nm for dielectric nickel–alumina composites, 0–60% nickel. The four data points were fitted with a second degree polynomial.

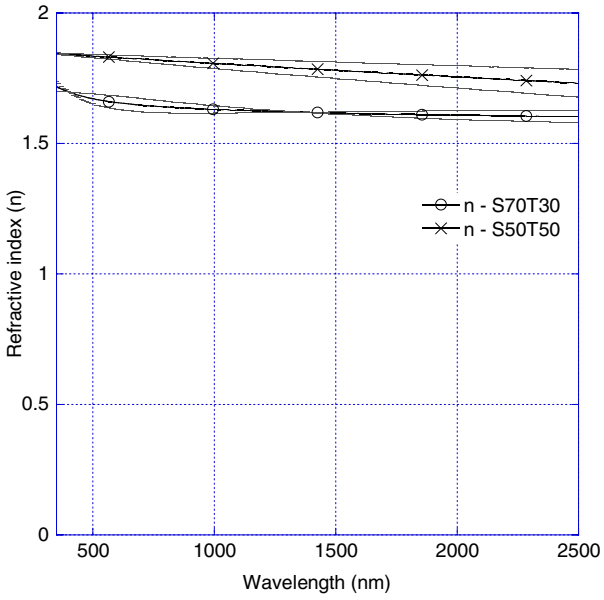

Figure 7. The real part (n) of the average refractive index of S70T30 and S50T50 thin film samples; the grey lines represent the standard deviation.

The refractive index of S70T30 is shown in figure 7. At 633 nm n equals 1.65 ± 0.02, which indicates that the S70T30 thin film in this study is slightly denser than Brusantin *et al* had found. An increasing amount of titania leads to a higher refractive index, as seen in figure 8. At 633 nm n equals 1.83 ± 0.01 for the S50T50 thin film. The complex refractive index for S70T30 and S50T50 can be seen in figure 8. All silica–titania samples were annealed to 500 °C.

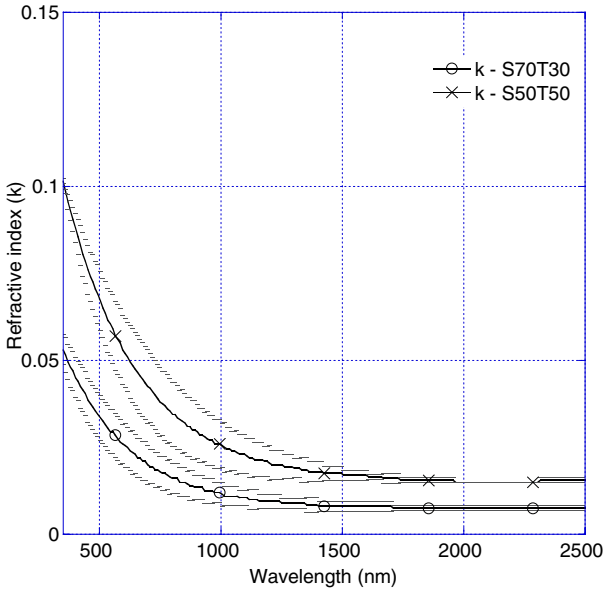

Figure 8. The imaginary part (k) of the average refractive index of S70T30 and S50T50 thin film samples; the grey lines represent the standard deviation.

5. Discussion

5.1. Optical constants

It would be interesting to make a Kramers–Krönig transformation of the results and hence check the reliability of the optical constants. However, since the refractive index information was only derived in such a short wavelength interval, 350–2500 nm, it is very difficult to make a reliable Kramers–Krönig transformation, and thus it was not done.

The derived optical constants for the silica, hybrid-silica, alumina and silica–titania thin film materials were, however, verified through references; see section 4. The solution-chemical processing method for the nickel–alumina composite presented here is novel but it is of interest to compare the optical properties of this material to similar nickel–alumina composites manufactured through other thin film deposition techniques.

What could be easily verified were the derived thicknesses from the thin film program. Reference white light interferometry thickness measurements normally showed a very good agreement, ± 3 nm. However, CODE seemed to slightly overestimate thicknesses of samples with 65 or 80% nickel, by up to 10 nm.

5.1.1. Nickel–alumina. Craighead *et al* [23] produced nickel–alumina composites using coevaporation of metal and dielectric. The nickel particles can be seen in transmission electron microscope images and the size is in the range 1–10 nm. Sathiaraj *et al* [24] manufactured nickel–alumina composites using RF sputtering with two composite targets. These sputtered nickel particles were very fine, too small to be resolved in an electron microscope. However, Sathiaraj *et al* do have confirmed crystalline nickel in the composite, verified by an electron diffractogram. The solution-chemically derived nickel–alumina composite studied in this paper has nickel particles ranging from about 5–10 nm and is hence more similar to the evaporated rather than the sputtered composite. Both Craighead *et al* and Sathiaraj *et al* have derived their

optical constants, separately at each measured wavelength in the interval 300–2500 nm, using reflectance and transmittance measurements and the Fresnel equations. The method applied in this paper was instead to use reflectance and transmittance measurements that were least square fitted over the whole measured interval, 350–2500 nm, using dispersion and Bruggeman models. The models generated the free parameters c_1–c_6, d and f which then were utilized to calculate the wavelength dependent optical constants.

Craighead *et al* have also modelled the refractive index using the Maxwell–Garnet (MG) theory and has found that this theory worked well for composites with metal volume fractions less than 0.2. Sathiaraj also modelled their composites but using both MG and Bruggeman theories. The latter found as well that the MG model worked well for volume fractions below 0.2, and the Bruggeman model only worked well for volume fractions around 0.4. Craighead *et al* present refractive index graphs with MG volume fractions between 0.14 and 0.39 [19, 23] which agree very well with N40A60 and N65A35 in figure 3. The n value at 2500 nm is 1.9 and 2.8 respectively for the two composites presented by Craighead *et al*. The corresponding n value for N40A60 is 1.99 ± 0.03 and 2.76 ± 0.17 for N65A35.

Sathiaraj *et al* present refractive index graphs with actual volume percentages of 0.21, 0.42, 0.57 and 0.61 [24]. These graphs do not agree that well with the derived optical constants found in this study. The largest difference lies in the extinction coefficient. Since the composites made by Sathiaraj do not have distinguishable metal particles there consequently is no absorption peak in k. Sathiaraj *et al* instead show a more or less constant k in the whole interval 300–2500 nm. As pointed out previously, figures 4 and 5 show clearly defined absorption peaks in k at around 500–700 nm deriving from the nickel nanoparticles.

It can be noted that the standard deviation increases with a nickel content of 65% or more. On looking in table 1, it can be seen that the volume fractions are very similar for samples with 60% nickel or less, in per cent units. But for the more metallic samples with 65 or 80% nickel the volume fraction varies to some degree. The increase in standard deviation can partly be explained by this variation in volume fraction. A variation in the volume fraction for high nickel percentage samples will especially affect the extinction coefficient. Accordingly the largest standard deviation is seen in the k value for N65A35 and N80A20.

5.1.2. Silica. A refractive index of 1.42, as found in this study, would according to Seco *et al* correspond to a porosity of about 8%. Elastic recoil detection analysis (ERDA) of the silica and hybrid-silica in this study has shown an organic carbon residue of about four atomic relative per cent for the silica thin films and 6% for the hybrid-silica, to be published in a pending paper. The lower n of 1.42, compared to 1.46, can partly be explained by the film porosity, but contaminants like carbon can also influence the refractive index. Depending on how the carbon atoms are bound in the silica structure they can either decrease or increase the refractive index. The imaginary part of the refractive index was equal to zero for both silica and hybrid-silica. A constant value was, however, not expected since the tabled value for dense amorphous silica (glass) is 1.48 at 350 nm and 1.43 at 2500 nm [12].

5.2. Volume fractions

The abbreviations NxxAyy in table 1 refer to volume percentages in the coating solution of nickel and alumina respectively, not in the solid resulting films. An ERDA of the studied nickel–alumina composites was made which show that the actual volume percentages in these films correspond well with the calculated solution volume percentages. On the other hand the calculated Bruggeman volume fractions derived from the fit and shown in table 1 correspond very poorly with real values. The reason for this mismatch lies partly in the Bruggeman model.

A Bruggeman volume fraction of about 35% or more according to the model means that the fill material has more or less percolated and the metal nickel particles would be in contact with each other. As a result of this percolation behaviour the optical properties according to the Bruggeman approximation would appear in this case very metallic for volume fractions over 35%. This behaviour was not found in the nickel–alumina composite studied here. Transmission electron images, even of the N80A20 material, show separated particles, also to be published in a pending paper [20].

Another reason for the disparity between real and model volume fractions would be due to highly dispersed nickel in the composite that changes the properties of the surrounding alumina matrix. Both Craighead *et al* and Sathiaraj *et al* suggest this theory. They also found that the Maxwell–Garnet model as well, just as the Bruggeman model, deviates from real volume fraction values, especially for medium to high volume fractions.

The alumina in the nickel–alumina composite studied was refitted and not taken from the previously modelled pure alumina. The motive for remodelling is because the properties of the alumina in the nickel–alumina composite change slightly with increasing nickel content. The amount of atomically dispersed nickel increases with increasing nickel content. The ERDA also shows that the stoichiometry changes: there is slightly more oxygen present than $3/2$ of the aluminium content for high nickel content composites. This indicates that the presence of small amounts of other oxides, such as NiO, Ni_2O_3, increases with increasing nickel content. It is therefore motivated to refit the alumina matrix for each sample. It was found that the fitting routine worked much better when remodelling the alumina for each individual nickel–alumina composite.

5.3. Solar absorber layer structure

Finally we briefly discuss how the derived optical constants were utilized. Knowing the refractive indices of the thin film materials in this study it was possible to design an optimized three-layer absorber. According to a thin film stack calculation program it should be composed of a highly absorbing N80A20 film of 100 nm at the base, a medium absorbing N40A60 film of 60 nm in the middle, and finally a pure dielectric silica or hybrid-silica film of 85 nm at the top [3]. The WLI reference thickness measurements, see section 4.1, were not made when [3] was written and hence the 80% nickel and the silica layer thicknesses are overestimated by about 20%.

An AR coating is most effective when its refractive index is equal to the square root of the refractive index of the material it is deposited on, which can be deduced from the Fresnel formula for thin films [25]. This formula is only valid for non-absorbing materials. The constant refractive index in near-infrared for the weakly absorbing mid N40A60 layer is 1.99. The square root of 1.99 is equal to 1.41, which corresponds well with the derived value for the AR material used, sol–gel derived thin film silica, which has a refractive index of 1.42 ± 0.02. The same calculation is not valid for the base and mid-layer because of the highly absorbing properties of the N80A20 material.

6. Conclusions

There are differences in the structure and hence the optical properties between the nickel–alumina composite materials described here, by Craighead *et al* and by Sathiaraj *et al*. The manufacturing method of a composite is important for the end properties of the material. The main differences lie in the metal particle size and shape, the density and the porosity of the composite and the amount of atomically dispersed nickel in the dielectric.

Fitting the optical constants of the alumina matrix for each individual nickel–alumina material as done in this study makes sense since the properties of the oxide change with varying nickel contents. The derived refractive indices found here could thus be more accurate compared to the work done by Craighead *et al* and Sathiaraj *et al* as they use the same tabled alumina refractive index for their varying composites. Concerning the refractive index of nickel, a tabled value of crystalline nickel was used in this study which can be justified by the fact that TEM investigations show crystalline nickel particles. However, the size of the particles does affect the refractive index.

Conclusively, the empirical mathematical model to derive optical properties of thin film materials from reflectance and transmittance measurements used in this article worked well. The refractive indices of nickel–alumina and silica–titania composites, alumina, silica and hybrid-silica were clearly stated and reproducible except for the nickel–alumina materials having a nickel content of 65% or more.

Acknowledgments

The authors would like to thank all members of the Solid State Physics group for their backing and encouragement. We would especially like to express our gratitude to Marco Schade for his help with the interferometer measurements. The work has been carried out under the auspices of The Energy Systems Program which is financed by the Swedish Energy Agency.

Appendix

Table A.1. Parameter values c_1 and c_2 for the Corning glass, see equation (1), and parameter values c_1–c_6 for all oxides related to the used dispersion model, see equation (2). The second subscript refers to the sample number, that is for N40A60 there are three samples.

Material	Corning	S/HS	S70T30	S50T50	A	N20A80	N40A60	N60A40	N65A35	N80A20
c_{11}	2.31	2.5×10^{-3}	4.3×10^{-1}	2.0	1.6×10^{-1}	2.8	2.8	4.1	4.0	3.7
c_{21}	0.17	2.9×10^{4}	9.9×10^{2}	7.3×10^{3}	7.0×10^{2}	1.7×10^{4}	6.7×10^{5}	3.5×10^{7}	4.5×10^{7}	1.1×10^{4}
c_{31}		2.1	2.5	1.3	2.5	15.7×10^{-3}	5.1×10^{-1}	8.7×10^{-3}	4.4×10^{-3}	11.0×10^{-4}
c_{41}		0	1.5×10^{-1}	3.2×10^{-1}	1.5×10^{-1}	2.8×10^{-1}	5.3×10^{-1}	4.3×10^{-1}	1.2	1.4
c_{51}		0	2.3×10^{2}	2.4×10^{2}	1.4×10^{2}	3.7×10^{2}	7.4×10^{2}	1.8×10^{2}	2.0×10^{2}	3.1×10^{2}
c_{61}		0	2.2×10^{-2}	5.3×10^{-2}	6.6×10^{-3}	6.4×10^{-2}	1.7×10^{-1}	8.7×10^{-1}	5.9×10^{-1}	50.0×10^{-4}
c_{12}		2.5×10^{-3}	3.7×10^{-1}	3.0	3.4×10^{-1}	3.0	3.0	3.9	4.1	3.1
c_{22}		3.1×10^{4}	1.4×10^{2}	22.3×10^{3}	1.3×10^{3}	1.9×10^{4}	11.6×10^{5}	3.7×10^{7}	4.5×10^{7}	2.1×10^{7}
c_{32}		1.9	2.6	0.4	2.4	8.3×10^{-3}	5.0×10^{-1}	9.8×10^{-3}	4.9×10^{-3}	0
c_{42}		0	1.7×10^{-1}	3.2×10^{-1}	2.2×10^{-1}	3.9×10^{-1}	6.2×10^{-1}	4.7×10^{-1}	1.6	1.4
c_{52}		0	3.0×10^{2}	3.9×10^{2}	2.3×10^{2}	3.4×10^{2}	6.7×10^{2}	1.6×10^{2}	2.2×10^{2}	3.1×10^{2}
c_{62}		0	2.6×10^{-2}	5.0×10^{-2}	13.5×10^{-3}	6.9×10^{-2}	1.6×10^{-1}	8.7×10^{-1}	5.0×10^{-1}	1.0×10^{-4}
c_{13}		2.7×10^{-3}				3.0	2.9		4.0	3.1
c_{23}		3.2×10^{4}				2.4×10^{4}	2.1×10^{5}		6.5×10^{7}	1.5×10^{4}
c_{33}		2.1				6.1×10^{-3}	5.6×10^{-1}		1.0×10^{-3}	7.0×10^{-4}
c_{43}		0				3.8×10^{-1}	6.2×10^{-1}		0.8	1.8
c_{53}		0				3.8×10^{2}	7.0×10^{2}		1.7×10^{2}	2.6×10^{2}
c_{63}		0				7.0×10^{-2}	1.7×10^{-1}		7.6×10^{-1}	1.0×10^{-4}
c_{14}		2.7×10^{-3}								2.7
c_{24}		3.2×10^{4}								1.3×10^{4}
c_{34}		2.0								88.0×10^{-4}
c_{44}		0								1.8
c_{54}		0								2.5×10^{2}
c_{64}		0								0

References

[1] Granqvist C G 1989 *Spectrally Selective Surfaces for Heating and Cooling Applications* (Washington: The International Society for Optical Engineering)

[2] Boström T, Wäckelgård E and Westin G 2003 Solution-chemical derived nickel–alumina coatings for thermal solar absorbers *Sol. Energy* **74** 497–504

[3] Boström T, Wäckelgård E and Westin G 2005 Experimental and theoretical optimization of a three layer solution chemically derived spectrally selective absorber *Proc. ISES (Orlando, 2005)*

[4] Theiss M 2002 *Hard and Software, CODE* Aachen, Germany

[5] Shuxi Z, Ribbing C-G and Wäckelgård E 2004 Optical constants of sputtered Ni/NiO solar absorber film-depth-profiled characterization *Sol. Energy Mater. Sol. Cells.* **84** 193–203

[6] Ward L 1998 *The Optical Constants of Bulk Materials and Films* (Great Britain: JW Arrowsmith Ltd)

[7] Tadanaga K, Iwashita K, Minami T and Tohge N 1996 Coating and water permeation properties of SiO2 thin films prepared by the sol–gel method on Nylon-6 substrates *J. Sol–Gel Sci. Technol.* **6** 107–11

[8] Duffie J A and Beckman W A 1991 *Solar Engineering of Thermal Processes* (New York: Wiley–Interscience)

[9] Paulick T C 1986 Inversion of normal-incidence (R,T) measurements to obtain $n + ik$ for thin films *Appl. Opt.* **25** 562–4

[10] Cauchy A L 1836 *Mémoire sur la Dispersion de la Lumière* Prague

[11] Bruggeman D A G 1935 Berechnung Verschiedener Physikalischer Konstanten von Heterogenen Substanzen *Ann. Phys.* **24** 636–64

[12] Palik E D 1985 *Handbook of Optical Constants of Solids* (Orlando, FL: Academic)

[13] Nelder J A and Mead R 1965 A simplex method for function minimization *Comput. J.* **7** 308–13

[14] Press W H, Teukolsky S A, Vetterling W T and Flannery B P 1992 *Numerical Recipes in FORTRAN: The Art of Scientific Computing* (Cambridge: Cambridge University Press)

[15] Dawnay E J C, Fardad M A, Green M, Horowitz F, Yeatman E M, Almeida R M, Vasconcelos H C, Guglielmi M and Martucci A 1995 Control and characterisation of microstructure in sol–gel films for optical device applications *Adv. Mater. Opt.* 55–62

[16] 2003 *Vin Karola Instruments* http://www.vinkarola.com Norcross

[17] Shamala K S, Murthy L C S and Narasimha Rao K 2004 Studies on optical and dielectric properties of Al2O3 thin films prepared by electron beam evaporation and spray pyrolysis method *Mater. Sci. Eng.* B **106** 269–74

[18] Eriksson T S, Hjortsberg A, Niklasson G A and Granqvist C G 1981 Infrared optical properties of evaporated alumina films *Appl. Opt.* **20** 2742–6

[19] Murr L E (ed) 1980 *Solar Materials Science* (London: Academic)

[20] Boström T, Valizadeh S, Lu J, Jensen J, Westin G and Wäckelgård E 2006 Characterizing a Ni-Al2O3/SiO2 solar thermal selective absorber *Thin Solid Films* submitted

[21] Seco A M, Goncalves M C and Almeida R M 2000 Densification of hybrid silica–titania sol–gel films studied by ellipsometry and FTIR *Mater. Sci. Eng.* B **76** 193–9

[22] Brusantin G, Guglielmi M, Innocenzi P, Martucci A, Battaglin G, Pelli S and Righini G 1997 Microstructural and optical properties of sol–gel silica–titania waveguides *J. Non-Cryst. Solids* **220** 202–9

[23] Craighead H G and Buhrman R A 1977 Optical properties of selectively absorbing Ni/Al2O3 composite films *Appl. Phys. Lett.* **31** 423–5

[24] Sathiaraj T and Thangaraj R 1997 The experimental and calculated optical properties of NI-Al2O3 coatings using effective medium theories *J. Phys. D: Appl. Phys.* **30** 769–75

[25] Meschede D 2002 *Gerthsen Physik* 21st edn (Berlin: Springer)